

A bound on Ekman pumping

Stephan R. de Roode^{1*}, A. Pier Siebesma^{1,2},

¹Delft University of Technology, The Netherlands.

²KNMI, De Bilt, The Netherlands.

Key Points:

- The large-scale vertical velocity caused by boundary-layer turbulent friction has a maximum value.

*Department of Geosciences and Remote Sensing, Faculty of Civil Engineering and Geosciences, Delft University of Technology, Stevinweg 1, 2628 CN Delft, The Netherlands

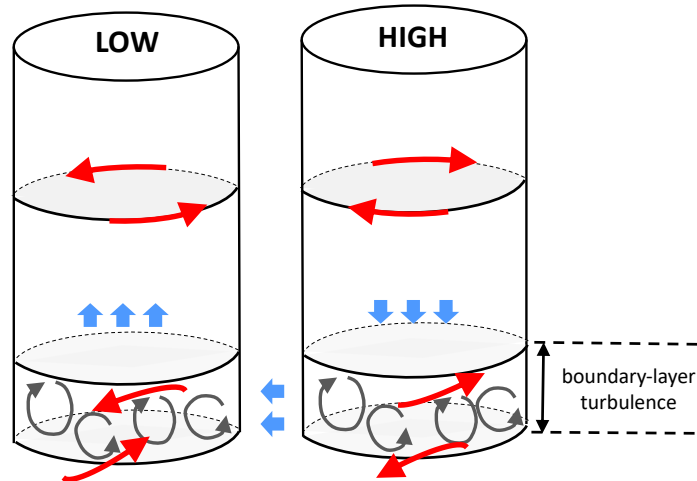
Corresponding author: S. R. de Roode, s.r.deroude@tudelft.nl

Abstract

Momentum transport by boundary-layer turbulence causes a weak synoptic-scale vertical motion. The classical textbook solution for the strength of this Ekman pumping depends on the curl of the surface momentum flux. A new solution for Ekman pumping is derived in terms of the curl of the geostrophic wind and a term that depends in a non-trivial way on the vertical profile of the turbulent momentum flux. The solution is confined to a boundary-layer regime that is vertically well mixed and horizontally homogeneous. The momentum flux is computed from a commonly used bulk surface drag formula and a flux-jump relation to capture the entrainment flux of momentum at the top of the boundary layer. It is found that the strength of Ekman pumping is bounded. The weakening of Ekman pumping for enhanced turbulent surface friction can be explained from the fact that it will reduce the magnitude of the horizontal wind. It is demonstrated that entrainment of momentum across the top of the boundary layer tends to diminish the large-scale divergence of the wind. As momentum transport is parameterized in large-scale models, the analysis is relevant for the understanding and interpretation of the evolution of synoptic-scale vertical motions as predicted by such models.

1 Introduction

Geostrophic flow is at the heart of dynamical meteorology. It elucidates why in a synoptic system of (low) high pressure on the northern hemisphere the wind vector is tangent to the isobars in a (counter-)clockwise direction. However, this theoretical wind structure is fully two-dimensional with a zero vertical velocity component. In fact, the presence of synoptic-scale vertical motion actually requires the consideration of turbulent boundary-layer eddies that act as a drag on the mean flow. As depicted schematically in Fig. 1, this friction effect gives rise to a net horizontal transport of air from high to low pressure. The resulting accumulation of mass drives a large-scale upwards vertical velocity in a low pressure system, and vice versa in a high pressure system. Because the magnitude of the turbulent friction controls the strength of the cross-isobaric flow [Svensson and Holtslag, 2009], it impacts the evolution of (anti) cyclones at synoptic scales [Sandu et al., 2013].



38 **Figure 1.** A schematic representation of Ekman pumping in a synoptic low and high pressure
 39 system (adapted from *Marshall and Plumb* [2016]). Boundary-layer eddies cause a cross-isobaric
 40 flow in which a net transport of air from high to low pressure occurs. This leads to a convergence
 41 of air in the low pressure system and a subsequent large-scale ascending motion. In the high
 42 pressure system large-scale subsidence is induced.

43 Although the characteristic synoptical-scale vertical velocity is small, typically on
 44 the order of cm s^{-1} , its effect on the evolution of the boundary layer cannot be neglected.
 45 Large-scale subsidence tends to advect the boundary-layer top downwards [*Lilly*, 1968],
 46 which has a strong impact on, for example, the concentration of air pollution in the at-
 47 mospheric boundary layer [*Seibert et al.*, 2000], the evolution of stratocumulus [*Zhang*
 48 *et al.*, 2009; *Van der Dussen et al.*, 2016], and Arctic mixed-phase stratocumulus [*Young*
 49 *et al.*, 2018]. On the other hand, convergence of air leads to an upward motion of air.
 50 Saturation of air, and subsequently clouds may develop as rising air cools down adiabat-
 51 ically. The generation of precipitation in such a system will be strongly controlled by the
 52 large-scale convergence [*Back and Bretherton*, 2009] .

Various efforts have been made to assess the large-scale subsidence from field ob-
 servations of horizontal wind and with use of the equation for conservation of mass,

$$\frac{\partial U}{\partial x} + \frac{\partial V}{\partial y} + \frac{\partial W}{\partial z} = 0, \quad (1)$$

with U , V , W the east-west (x), north-south (y) and vertical (z) components of the wind vector, respectively. The mean vertical velocity is controlled by the large-scale divergence of horizontal wind,

$$D \equiv \left(\frac{\partial U}{\partial x} + \frac{\partial V}{\partial y} \right) = -\frac{\partial W}{\partial z}. \quad (2)$$

53 This diagnostic expression proved useful to study the diurnal cycle of D from radioson-
 54 des that were launched during the Atlantic Stratocumulus Transition EXperiment (AS-
 55 TEX) [Ciesielski *et al.*, 1999]. Lenschow *et al.* [2007] studied aircraft measurements of
 56 the horizontal wind field collected from circular legs flown during the Second Dynam-
 57 ics and Chemistry of Marine Stratocumulus (DYCOMS-II) experiment and they con-
 58 cluded that this measurement strategy is not suitable to diagnose D as it yields unac-
 59 ceptable large errors. By contrast, from a careful analysis of observations from dropson-
 60 des that were released from an aircraft that flew along circular patterns over the trop-
 61 ical Atlantic near Barbados Bony *et al.* [2017] demonstrated that this strategy can ac-
 62 tually be rather well used to determine D with a sufficient accuracy.

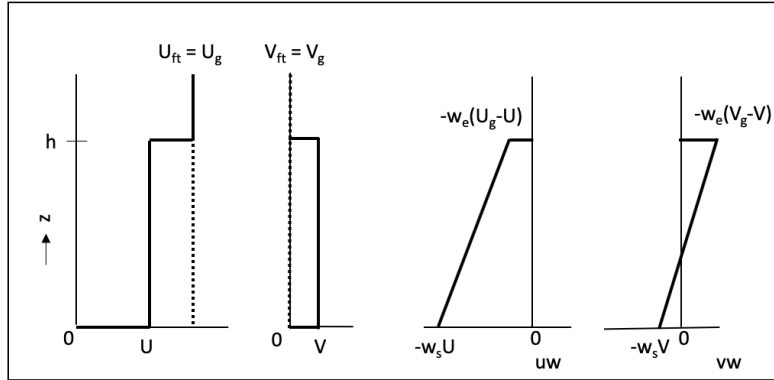
63 A well known and frequently used solution for the mean vertical motion depends
 64 on the curl of the surface momentum flux [Beare, 2007]. In this note a new diagnostic
 65 equation for the large-scale divergence of the horizontal wind D in terms of the strength
 66 of a non-dimensional turbulent boundary-layer friction factor and entrainment of mo-
 67 mentum across the top of the boundary layer will be derived. It will be demonstrated
 68 that this solution predicts a maximum value for the large-scale divergence of the hor-
 69 izontal wind.

70 **2 Theory**

71 The dependency of the large-scale vertical velocity on the momentum flux profile
 72 can be readily obtained from the conservation equations for momentum and mass. The
 73 main goal of this note is to study the effect of boundary-layer friction on Ekman pump-
 74 ing. To this end we will consider an idealized steady-state, horizontally homogeneous and
 75 vertically well-mixed boundary-layer forced by a constant geostrophic wind. The mo-
 76 mentum flux will be specified in terms of a bulk surface friction factor and an entrain-
 77 ment velocity at the top of the boundary layer.

78 The mixed-layer model framework originally developed by Stevens *et al.* [2002] is
 79 depicted schematically in Fig. 2. The horizontal wind is constant with height in the bound-

80 ary layer. This approximation holds rather well for convectively driven atmospheric bound-
 81 ary layers. Further support for the use of this model is given by *Back and Bretherton*
 82 [2009] who showed that it can skilfully reproduce observed surface winds and convergence
 83 over the tropical oceans.



84 **Figure 2.** A schematic representation of the vertical profiles of the steady-state horizontal
 85 wind components and their vertical turbulent fluxes (thick black lines) for a forcing $U_g > 0$ (indi-
 86 cated by the black dotted vertical line) and $V_g = 0$. The momentum fluxes at the surface and at
 87 the top of the boundary layer are computed with bulk formulae.

88 2.1 Governing equations

The horizontal momentum equations read,

$$\frac{dU}{dt} = fV - \frac{1}{\rho} \frac{\partial P}{\partial x} - \frac{\partial \overline{uw}}{\partial z}, \quad (3)$$

$$\frac{dV}{dt} = -fU - \frac{1}{\rho} \frac{\partial P}{\partial y} - \frac{\partial \overline{vw}}{\partial z}, \quad (4)$$

89 with P the pressure, f the Coriolis parameter, and \overline{uw} and \overline{vw} the Reynolds averaged
 90 momentum fluxes. Due to our assumption of horizontal homogeneity the mean horizon-
 91 tal advection terms vanish. Mean vertical advection of momentum is zero as in the bound-
 92 ary layer the wind is assumed to be constant with height. Last, we will use a constant
 93 value for the density of air ρ .

In the absence of turbulence a geostrophic balance is maintained by the Coriolis
 and the pressure gradient forces,

$$U = U_g \equiv -\frac{1}{\rho f} \frac{\partial P}{\partial y}, \quad V = V_g \equiv \frac{1}{\rho f} \frac{\partial P}{\partial x}, \quad (5)$$

94 with U_g and V_g defining the geostrophic wind velocity components. The fact that a purely
 95 geostrophic flow does not support any mean vertical motion can be derived from a sub-
 96 stitution of the geostrophic solution Eq. (5) in Eq. (2) which gives $D = 0$.

The importance of turbulence on the vertical motion becomes clear after a differ-
 entiation of Eqs. (3) and (4) with respect to y and x , respectively, and the use of these
 expressions in Eq. (2),

$$-\frac{\partial}{\partial z} \left[fW - \frac{\partial \overline{uw}}{\partial y} + \frac{\partial \overline{vw}}{\partial x} \right] = 0. \quad (6)$$

Here we reversed the order of differentiation in the pressure and momentum flux terms.
 The latitudinal variation of the Coriolis parameter $\partial f / \partial y$ will be ignored. The vertical
 gradient of W has entered equation (6) by the use of the continuity equation (1). A ver-
 tical integration from the surface (indicated by the subscript 'sfc') upwards to the height
 h^+ , which is just above the boundary layer where turbulence vanishes, shows that the
 vertical velocity depends on the curl of the surface momentum fluxes [Beare, 2007],

$$W|_{h^+} = \frac{1}{f} \left(\frac{\partial \overline{uw}_{\text{sfc}}}{\partial y} - \frac{\partial \overline{vw}_{\text{sfc}}}{\partial x} \right), \quad (7)$$

97 with $W = 0$ at the ground surface. The vertical velocity that is driven by surface mo-
 98 mentum fluxes is called Ekman pumping after the Swedish oceanographer who was the
 99 first to derive an analytical solution for wind-driven horizontal transport in the ocean.
 100 Ekman's solution for ocean flow is widely used as a powerful diagnostic tool that relates
 101 the strength of Ekman pumping in the ocean to the curl of the wind stress exerted at
 102 the Ocean's surface. Note that Eq. (7) ignores the effect of entrainment fluxes at the top
 103 of the boundary layer. To further explore the role of the momentum fluxes on Ekman
 104 pumping we will now apply parameterizations for their values at the surface and at the
 105 top of the boundary layer due to entrainment.

106 2.2 Parameterization of the momentum flux

The surface momentum fluxes can be expressed by the following bulk formula,

$$(\overline{uw}_{\text{sfc}}, \overline{vw}_{\text{sfc}}) = -C_d U_{\text{spd}} (U, V), \quad (8)$$

with U_{spd} the wind speed,

$$U_{\text{spd}} = \sqrt{U^2 + V^2}. \quad (9)$$

The factor C_d is turbulent drag coefficient that depends on the vertical stability and the
 roughness length [Schröter et al., 2013]. Because the magnitude of U_{spd} is controlled by

the surface drag coefficient C_d , the parameterization of the surface momentum flux has introduced a non-linearity in the system. To avoid this additional complexity, the formulation of the surface momentum flux may be further simplified by introducing a linearized friction coefficient [Back and Bretherton, 2009],

$$w_{\text{sfc}} = C_d U_{\text{spd}}. \quad (10)$$

107 This factor is sometimes referred to as a surface ventilation velocity.

The flux at the top of the boundary layer, denoted by h , can be expressed by the 'flux-jump' relation in a similar fashion [Lilly, 1968],

$$\overline{uw}_h = -w_e(U_{\text{ft}} - U) \quad , \quad \overline{vw}_h = -w_e(V_{\text{ft}} - V), \quad (11)$$

with w_e the entrainment velocity, and the subscript 'ft' represents the value of free tropospheric value of the wind just above the boundary layer. In the remainder we will assume that the wind in the free troposphere is in a geostrophic balance, $(U_{\text{ft}}, V_{\text{ft}}) = (U_g, V_g)$. Because both the actual and geostrophic winds are assumed to be constant with height in the boundary layer, the condition of a steady state requires that the momentum flux must vary linearly with height in order to balance their net force, which allows to express the vertical change of the momentum fluxes as follows,

$$\frac{\partial \overline{uw}}{\partial z} = \frac{-w_e(U_g - U) + w_{\text{sfc}}U}{h} \quad , \quad \frac{\partial \overline{vw}}{\partial z} = \frac{-w_e(V_g - V) + w_{\text{sfc}}V}{h}, \quad (12)$$

to give the following momentum balance equations,

$$\begin{aligned} V - V_g + k_{\text{top}}U_g - (k_{\text{sfc}} + k_{\text{top}})U &= 0, \\ -U + U_g + k_{\text{top}}V_g - (k_{\text{sfc}} + k_{\text{top}})V &= 0. \end{aligned} \quad (13)$$

Here we introduced the non-dimensional factors,

$$k_{\text{sfc}} = \frac{w_{\text{sfc}}}{fh} \quad , \quad k_{\text{top}} = \frac{w_e}{fh}. \quad (14)$$

108 The factor k_{sfc} may be interpreted as a turbulent Ekman number as it compares the im-
109 portance of surface ("viscous") friction relative to the Coriolis force.

110 The use of the factor w_{sfc} enables us to solve U and V analytically from Eq. (13).
111 In the next section we will effectively apply this strategy. This is motivated by the fact
112 that the analytical solutions for the boundary-layer wind, and more specifically their de-
113 pendency on the non-dimensional factors k_{sfc} and k_{top} , will demonstrate some impor-
114 tant general behaviour of Ekman pumping. However, in section 3.3 we will discuss an
115 example that is based on numerical solutions of the momentum equations for a prescribed
116 value of the bulk surface friction C_d .

117 **3 Analytical solutions for the large-scale divergence and subsidence**

118 Here we present and discuss the analytical solutions for the large-scale flow that
119 follow from the steady-state linearized momentum equations (13).

120 **3.1 Analytical steady-state solutions**

The solutions for the horizontal wind can be expressed in terms of the geostrophic wind,

$$\begin{aligned} U &= \frac{1 + k_{\text{top}}(k_{\text{sfc}} + k_{\text{top}})}{1 + (k_{\text{sfc}} + k_{\text{top}})^2} U_{\text{g}} - \frac{k_{\text{sfc}}}{1 + (k_{\text{sfc}} + k_{\text{top}})^2} V_{\text{g}}, \\ V &= \frac{1 + k_{\text{top}}(k_{\text{sfc}} + k_{\text{top}})}{1 + (k_{\text{sfc}} + k_{\text{top}})^2} V_{\text{g}} + \frac{k_{\text{sfc}}}{1 + (k_{\text{sfc}} + k_{\text{top}})^2} U_{\text{g}}. \end{aligned} \quad (15)$$

The divergence of the horizontal wind field can be obtained with aid of Eq. (2),

$$D = F(k_{\text{sfc}}, k_{\text{top}}) \left(\frac{\partial U_{\text{g}}}{\partial y} - \frac{\partial V_{\text{g}}}{\partial x} \right) = -F(k_{\text{sfc}}, k_{\text{top}}) \frac{\nabla^2 P}{\rho f}, \quad (16)$$

where we introduced the function

$$F(k_{\text{sfc}}, k_{\text{top}}) = \frac{k_{\text{sfc}}}{1 + (k_{\text{sfc}} + k_{\text{top}})^2}, \quad (17)$$

and ∇ indicates the Laplacian operator in the horizontal directions. The function F is also present in the solution for the large-scale vertical velocity, whose magnitude at the top of the boundary layer can be readily obtained from a vertical integration of D ,

$$w|_h = -F(k_{\text{sfc}}, k_{\text{top}}) \left(\frac{\partial U_{\text{g}}}{\partial y} - \frac{\partial V_{\text{g}}}{\partial x} \right) h, \quad (18)$$

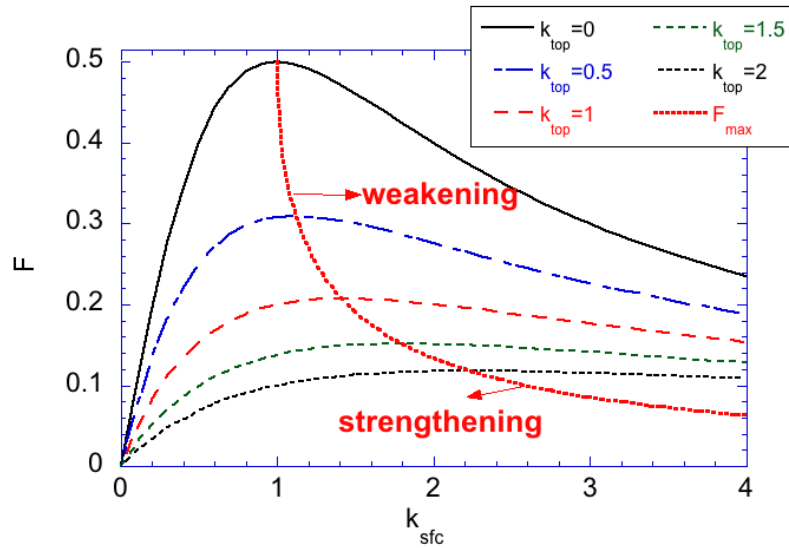
121 where we assumed that the value of D is constant within the boundary layer, which is
122 not an uncommon assumption for vertically well-mixed boundary layers [*Stevens, 2006*].

123 **3.2 Interpretation**

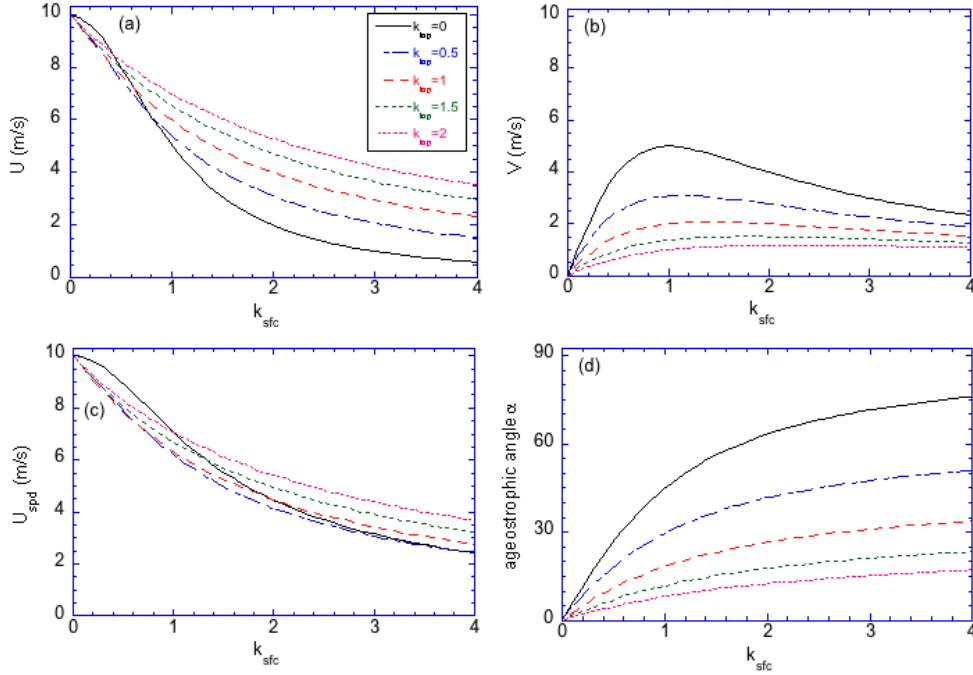
124 The solutions for the mean vertical velocity (7) and (18) differ in the sense that the
125 former depends on the curl of the surface momentum flux, whereas the new solution Eq.
126 (18) depends on the curl of the geostrophic wind, or, alternatively, on the Laplacian of
127 the pressure field. One might be tempted to hypothesize that a larger surface friction
128 will yield a stronger Ekman pumping from the premise that more surface friction will
129 cause an enhancement of the surface momentum flux. We will now argue that k_{sfc} puts
130 a bound on the strength of Ekman pumping, a condition that cannot be inferred directly
131 from Eq. (7).

132 **3.2.1 Surface friction effect, no entrainment ($k_{\text{top}} = 0$)**

133 Let us inspect the function F shown in Fig. 3. For a frictionless flow, $k_{\text{sfc}} = k_{\text{top}} =$
 134 0, we recover the solutions of a geostrophic balance (5), and consequently there will be
 135 no large-scale divergence since $F = 0$. For $k_{\text{sfc}} > 0$ we find that $V > 0$, which indi-
 136 cates that cross-isobaric flow occurs. The presence of this ageostrophic wind component
 137 results in the large-scale divergence (or convergence) of the flow that, in turn, drives the
 138 large-scale vertical motions. If the surface friction goes to infinity, or equivalently, $k_{\text{sfc}} \rightarrow$
 139 ∞ , then $F \rightarrow 0$. In this limit surface friction damps the horizontal wind to zero, and
 140 subsequently the large-scale divergence $D \rightarrow 0$. This leads to the key conclusion that
 141 the effect of surface friction on the large-scale vertical velocity is bounded. Eq. (17) pre-
 142 dicted that the large-scale divergence is maximum with $F = 1$ for $k_{\text{sfc}} = 1$ and zero en-
 143 trainment, $k_{\text{top}} = 0$. According to Eq. (15) this solution corresponds to $U = V =$
 144 $\frac{1}{2}U_g$, and since the angle of the actual wind with the geostrophic wind is given by $\tan \alpha =$
 145 V/U we find this so-called ageostrophic angle to be equal to $\alpha = 45^\circ$.



146 **Figure 3.** The factor F as a function of the non-dimensional surface friction (k_{sfc}) and en-
 147 trainment (k_{top}) factors as defined by Eq. (17). The red dotted line connects the maximum
 148 values for the function F . The regime left of the red dotted line is indicated by 'strengthening',
 149 which means that the large-scale divergence D increases for increasing k_{sfc} . In the weakening
 150 regime, D will decrease for increasing k_{sfc} . The linestyles are according to the legend.



151 **Figure 4.** The wind component (a) U , (b) V , (c) wind speed U_{spd} and (d) the ageostrophic
 152 angle α as a function of the non-dimensional surface friction (k_{sfc}) and entrainment (k_{top}) factors
 153 as defined by Eq. (17) for $U_g = 10 \text{ ms}^{-1}$ and $V_g = 0$. The linestyles are according to the legend.

154 3.2.2 Combined surface friction and entrainment

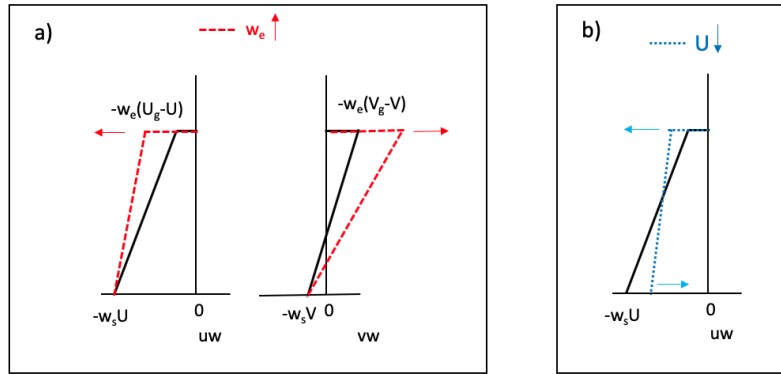
Before discussing the large-scale divergence let us first discuss the solutions for the horizontal wind according to Eq. (15), which show that in the presence of turbulence the steady-state wind speed becomes

$$U_{\text{spd}}^2 = \frac{1 + k_{\text{top}}^2}{1 + (k_{\text{sfc}} + k_{\text{top}})^2} (U_g^2 + V_g^2) \leq |\vec{U}_g|^2. \quad (19)$$

155 Surface friction and entrainment appear to have opposing effects on the wind speed. This
 156 can be seen from the limit $k_{\text{sfc}} \rightarrow \infty$ which yields a zero wind speed. By contrast, for
 157 strong entrainment the free tropospheric wind speed is imposed on the boundary layer,
 158 as for $k_{\text{top}} \rightarrow \infty$ we find $U_{\text{spd}} \rightarrow |\vec{U}_g|$.

159 Fig. 4 shows examples of U , V , U_{spd} and the ageostrophic angle α for a forcing $U_g =$
 160 10 ms^{-1} and $V_g = 0$. While V tends to become smaller with increasing entrainment
 161 velocity, we notice a more delicate dependency of U on entrainment in the sense that for
 162 small (large) k_{sfc} , U tends to decrease (increase) for increasing entrainment velocity. This

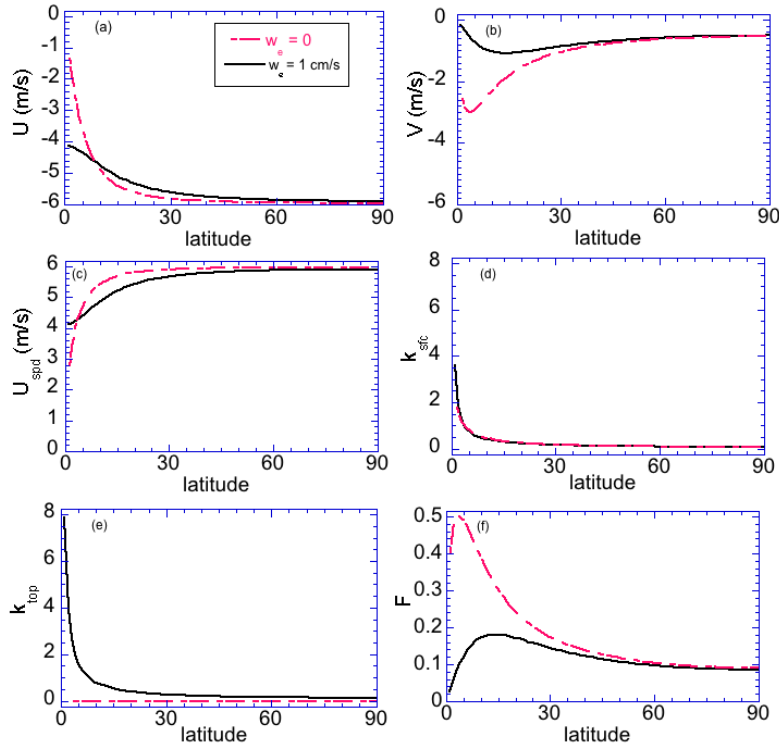
163 results in a wind speed U_{spd} that tends to diminish for increasing entrainment in the regime
 164 $k_{\text{sfc}} < 2/k_{\text{top}}$. *Stevens et al.* [2002] explains that this is caused by an asymmetry in the
 165 entrainment flux. Fig. 5 illustrates that entrainment tends to enhance the momentum
 166 fluxes at the top of the boundary layer which results, however, in opposing effects on the
 167 vertical gradients of \overline{uw} and \overline{vw} . If the vertical slope of \overline{vw} is enhanced by a larger en-
 168 trainment velocity, there will be a stronger damping acting on V by turbulent friction,
 169 which results in a smaller steady-state value of V , in accord with the results displayed
 170 in Fig. 4. As a consequence, the forcing term fV that is present in the budget equation
 171 (3) for U is also reduced, and to achieve a steady-state the vertical slope of \overline{uw} has to
 172 diminish. An increase in the entrainment velocity can already partly support this, but
 173 if this does not yield the requested total change in the vertical gradient of \overline{uw} a balance
 174 can be achieved only if U is decreased as well.



175 **Figure 5.** A schematic representation of the effect of a) an increase in the entrainment ve-
 176 locity (red dashed lines) w_e and b) a decrease of the horizontal wind component U (blue dotted
 177 line) on the momentum flux profiles. The black lines indicate the momentum flux profiles belong-
 178 ing to a steady-state solution for a forcing $U_g > 0$ and $V_g = 0$ as shown in Fig. 2. An increase in
 179 entrainment causes a larger slope of \overline{vw} (stronger effect of turbulent friction) but a smaller slope
 180 of \overline{uw} (smaller effect of turbulent friction).

An important consequence of the presence of entrainment is that it tends to dimin-
 ish the large-scale divergence (see Fig. 3). Moreover, the maximum value of F is shifted
 towards larger values of k_{sfc} . This can be derived by setting the derivative of the func-
 tion F with respect to k_{sfc} to zero to give,

$$k_{\text{sfc}} = \sqrt{1 + k_{\text{top}}^2}. \quad (20)$$



181 **Figure 6.** Numerical solutions for the wind velocity (a) U , (b) V , (c) the wind speed U_{spd} ,
 182 the non-dimensional (d) surface friction factor k_{sf} , the entrainment factor (e) k_{top} , and (f) the
 183 function F as a function of the latitude. The forcing conditions were taken from *Stevens et al.*
 184 [2002], $C_d = 0.00111$, $U_g = -6 \text{ ms}^{-1}$, $h = 500 \text{ m}$. The results for the wind as obtained for an
 185 entrainment velocity of 1 cm s^{-1} are identical to his Figure 1, and the zero entrainment case is
 186 added here to illustrate its impact on the wind. The linestyles are according to the legend.

187 3.3 A numerical example for a case with a prescribed bulk surface drag 188 coefficient C_d

189 As a practical illustration of the theory we took the reference case of *Stevens et al.*
 190 [2002], with $h = 500 \text{ m}$, $w_e = 1 \text{ cm s}^{-1}$, $U_g = 6 \text{ ms}^{-1}$. Furthermore C_d is set to 0.0011
 191 which is a typical value over the tropical oceans. However, noting that the relevant pa-
 192 rameters k_{sf} and k_{top} do both depend on reciprocal of the Coriolis parameter we have
 193 computed results up to a latitude of 90° . The sensitivity of the results on the entrain-
 194 ment is addressed by setting w_e to zero. Because U_{spd} depends on the prescribed value
 195 of C_d , the solutions shown in Fig. 6 were computed numerically, and as a consequence
 196 the bulk surface friction factor k_{sf} , that is now diagnosed from the resulting wind speed

197 according to $k_{\text{sfc}} = C_d U_{\text{spd}}/hf$, differs for the two cases shown. Except for a narrow
 198 band near the tropics, where k_{sfc} exceeds unity, entrainment tends to diminish the wind
 199 speed. The wind speed tends to approach the (absolute) value of the geostrophic wind
 200 towards higher latitudes. This can be explained from the bulk surface friction factor k_{sfc}
 201 whose magnitude diminishes away from the Equator. The effect of entrainment on Ek-
 202 man pumping is evident from the resulting shape of the function F which in the trop-
 203 ical regime is diminished by more than a factor of about two with respect to the case
 204 without entrainment. In conclusion, the findings suggest that maximum values for the
 205 function F are most likely to be expected at low latitudes.

206 3.4 Discussion

207 *Sandu et al.* [2013] evaluated the effect of a less diffusive parameterization for tur-
 208 bulent transport in stably-stratified boundary layers in the European Centre for Medium-
 209 Range Weather Forecasts (ECMWF) model, and confirmed that the strength of turbu-
 210 lence diffusion affects the large-scale flow by modulating the strength of synoptic-scale
 211 systems. Moreover, they found that the model improved the representation of high-pressure
 212 systems, but the storm track region in the Southern Hemisphere was less well captured.
 213 Our analysis suggests that the question as to which a change in the parameterization of
 214 turbulence in a large-scale weather forecast model leads to either a strengthening or a
 215 weakening effect on the evolution of synoptic-scale systems, depends on the factors k_{sfc}
 216 and k_{top} in a nontrivial way.

217 It should be noted that the boundary-layer depth itself is controlled by the strength
 218 of turbulence. For example, the enhancement of turbulent diffusion in stable conditions,
 219 used to improve the representation of large-scale synoptic systems, leads not only to larger
 220 momentum fluxes but also to deeper boundary-layers [*Sandu et al.*, 2013; *Svensson and*
 221 *Holtslag*, 2009]. For the case studied here, a larger entrainment rate will cause a deeper
 222 boundary layer, which according to Eq. (18) will enhance Ekman pumping since cross-
 223 isobaric flow will take place over a deeper layer depth h . However, entrainment has an
 224 opposing impact on Ekman pumping via its control on the function F . In particular, if
 225 the modelled entrainment is too large, the function F will become smaller as shown in
 226 Fig. 3. This suggests that a bias in the entrainment in convective well mixed bound-
 227 ary layers may yield only a limited impact on Ekman pumping.

4 Conclusion

The present study discusses the effect of boundary-layer turbulence on the magnitude of the large-scale vertical velocity. In particular, a vertically well-mixed and horizontally homogeneous structure of the boundary layer is assumed. We confine our analysis to steady-state conditions and we use bulk parameterizations following the mixed layer model for wind as used in *Stevens et al.* [2002]. We present new diagnostic relations for the large-scale divergence of horizontal wind (D) and the large-scale vertical velocity.

In the absence of entrainment a maximum value for the large-scale divergence D is found if the non-dimensional surface friction factor k_{sfc} is equal to unity, a value which corresponds to a situation in which the actual wind has a cross-isobaric (ageostrophic) angle of 45° . The factor k_{sfc} can be thought of as an Ekman number that weighs the importance of the turbulent surface momentum flux relative to the force due to planetary rotation. A maximum value of Ekman pumping can be explained from the following notion. For a purely frictionless geostrophic flow the large-scale divergence of horizontal wind $D = 0$ and consequently there will be no Ekman pumping. The presence of surface friction act as a drag on the flow that generates an ageostrophic flow component giving $D \neq 0$, which, in turn, drives a small large-scale velocity. However, in the limit of infinite turbulent surface friction the horizontal wind will tend to zero, and likewise $D = 0$. This reasoning suggests a maximum effect of turbulent surface friction on the magnitude of D , which is quantified in this study. More precisely, D is found to depend on the curl of the geostrophic wind, in addition to a function F that depends on the non-dimensional factors related to surface friction and entrainment. It is found that entrainment tends to diminish the large-scale divergence.

The findings reported in this note might be useful to fine-tune parameterizations in global models such as explored in the study by *Sandu et al.* [2013] and including the ones which apply an explicit formulation of turbulent form drag due to subgrid orography [*Beljaars et al.*, 2004], or to better understand the impact of the parameterization of the bulk drag coefficient C_d on the model outcome [*Moon et al.*, 2007; *Foreman and Emeis*, 2010]. However, our study is restricted to vertically well mixed layers, a condition that is not applicable to the nocturnal stable boundary layer whose structure exhibits strong vertical gradients.

260 In the context of the present analysis it is worthwhile to mention some relevant stud-
261 ies on Ekman pumping based on height-dependent solutions for the wind by *Wu and Blu-*
262 *men* [1982] and *Tan* [2001]. *Wu and Blumen* derived analytical solutions for the boundary-
263 layer wind profile for non-stationary conditions. They maintained the advective trans-
264 port term in the momentum equation, and they parameterized the momentum flux with
265 a downgradient diffusion approach. Their solution is a modified Ekman spiral, a solu-
266 tion that closely mimics the one that is frequently observed for stable boundary layers,
267 with the wind direction and wind speed depending on the magnitude of the constant eddy
268 viscosity. *Tan* [2001] investigated the role of a height-dependent eddy viscosity and a baro-
269 clinic pressure field on Ekman pumping from an analysis of an approximate solution for
270 the wind. *Tan* concluded that a variable eddy viscosity and inertial acceleration have
271 an important role in the divergence in the boundary layer and the subsequent Ekman
272 pumping strength. A similar analysis might be performed for a clear convective boundary-
273 layer regime. For example, *Stevens et al.* [2002] presented height-dependent wind pro-
274 files as obtained with a turbulent diffusion parameterization.

275 Acknowledgements

276 We thank one anonymous reviewer and Dr. Anton Beljaars for some critical yet
277 constructive comments which motivated to perform the analysis from a mixed-layer frame-
278 work including entrainment. We also Drs. Bert Holtslag, Harm Jonker and Bas van de
279 Wiel for interesting discussions.

280 References

- 281 Back, L. E., and C. S. Bretherton (2009), On the relationship between sst gradients,
282 boundary layer winds, and convergence over the tropical oceans, *J. Clim.*, *22*(15),
283 4182–4196.
- 284 Beare, R. J. (2007), Boundary layer mechanisms in extratropical cyclones, *Q. J. R.*
285 *Meteorol. Soc.*, *133*(623), 503–515.
- 286 Beljaars, A. C., A. R. Brown, and N. Wood (2004), A new parametrization of turbu-
287 lent orographic form drag, *Q. J. R. Meteorol. Soc.*, *130*(599), 1327–1347.
- 288 Bony, S., B. Stevens, F. Ament, S. Bigorre, P. Chazette, S. Crewell, J. Delanoë,
289 K. Emanuel, D. Farrell, C. Flamant, S. Gross, L. Hirsch, J. Karstensen, B. Mayer,
290 L. Nuijens, J. H. Ruppert, I. Sandu, P. Siebesma, S. Speich, F. Szczap, J. Totems,

- 291 R. Vogel, M. Wendisch, and M. Wirth (2017), EUREC4A: A field campaign to
 292 elucidate the couplings between clouds, convection and circulation, *Surveys in*
 293 *Geophysics*, *38*(6), 1529–1568, doi:10.1007/s10712-017-9428-0.
- 294 Ciesielski, P. E., W. H. Schubert, and R. H. Johnson (1999), Large-scale heat and
 295 moisture budgets over the ASTEX region, *J. Atmos. Sci.*, *56*(18), 3241–3261.
- 296 Foreman, R. J., and S. Emeis (2010), Revisiting the definition of the drag coeffi-
 297 cient in the marine atmospheric boundary layer, *Journal of physical oceanography*,
 298 *40*(10), 2325–2332.
- 299 Lenschow, D. H., V. Savic-Jovicic, and B. Stevens (2007), Divergence and vortic-
 300 ity from aircraft air motion measurements, *J. Atmos. Ocean. Technol.*, *24*(12),
 301 2062–2072.
- 302 Lilly, D. (1968), Models of cloud-topped mixed layers under a strong inversion, *Q. J.*
 303 *R. Meteorol. Soc.*, *94*, 292–309.
- 304 Marshall, J., and R. A. Plumb (2016), *Atmosphere, ocean and climate dynamics: An*
 305 *introductory text*, vol. 21, Academic Press.
- 306 Moon, I.-J., I. Ginis, T. Hara, and B. Thomas (2007), A physics-based parameteri-
 307 zation of air–sea momentum flux at high wind speeds and its impact on hurricane
 308 intensity predictions, *Mon. Weather Rev.*, *135*(8), 2869–2878.
- 309 Sandu, I., A. Beljaars, P. Bechtold, T. Mauritsen, and G. Balsamo (2013), Why is it
 310 so difficult to represent stably stratified conditions in numerical weather prediction
 311 (NWP) models?, *J. Adv. Model Earth Syst.*, *5*(2), 117–133.
- 312 Schröter, J. S., A. F. Moene, and A. A. Holtslag (2013), Convective boundary layer
 313 wind dynamics and inertial oscillations: the influence of surface stress, *Q. J. R.*
 314 *Meteorol. Soc.*, *139*(676), 1694–1711.
- 315 Seibert, P., F. Beyrich, S.-E. Gryning, S. Joffre, A. Rasmussen, and P. Tercier
 316 (2000), Review and intercomparison of operational methods for the determina-
 317 tion of the mixing height, *Atmos Environ*, *34*(7), 1001–1027.
- 318 Stevens, B. (2006), Bulk boundary-layer concepts for simplified models of tropical
 319 dynamics, *Theor. Comput. Fluid. Dyn.*, doi:DOI10.1007/s00162-006-0032-z.
- 320 Stevens, B., J. Duan, J. C. McWilliams, M. Münnich, and J. D. Neelin (2002), En-
 321 trainment, rayleigh friction, and boundary layer winds over the tropical pacific, *J.*
 322 *Clim.*, *15*(1), 30–44.

- 323 Svensson, G., and A. A. Holtslag (2009), Analysis of model results for the turning of
324 the wind and related momentum fluxes in the stable boundary layer, *Boundary-*
325 *Layer Meteorol.*, *132*(2), 261–277.
- 326 Tan, Z.-M. (2001), An approximate analytical solution for the baroclinic and vari-
327 able eddy diffusivity semi-geostrophic Ekman boundary layer, *Boundary-Layer*
328 *Meteorol.*, *98*(3), 361–385.
- 329 Van der Dussen, J. J., S. R. de Roode, and A. P. Siebesma (2016), How large-scale
330 subsidence affects stratocumulus transitions, *Atmos. Chem. Phys.*, *16*, 691–701.
- 331 Wu, R., and W. Blumen (1982), An analysis of Ekman boundary layer dynamics
332 incorporating the geostrophic momentum approximation, *J. Atmos. Sci.*, *39*(8),
333 1774–1782.
- 334 Young, G., P. J. Connolly, C. Dearden, and T. W. Choullarton (2018), Relating
335 large-scale subsidence to convection development in Arctic mixed-phase marine
336 stratocumulus, *Atmos Chem Phys.*, *18*, 1475–1494.
- 337 Zhang, Y., B. Stevens, B. Medeiros, and M. Ghil (2009), Low-cloud fraction, lower-
338 tropospheric stability, and large-scale divergence, *J. Clim.*, *22*(18), 4827–4844.